Application of the boundary element method for numerical modelling of the seismic hazard at Bambanani gold mine in South Africa

by J. Gerber[1,3], N. de Koker[1], Y Jooste[2]

Affiliation:
[1]Stellenbosch University, South Africa
[2]Harmony Gold Mine, South Africa
[3]Institute of Mine Seismology, South Africa

Correspondence to:
J. Gerber

Email:
Jacques.Gerber@IMSeismology.org

Dates:
Received: 14 Jul. 2025
Published: November 2025

How to cite:
Gerber, J., De Koker, N., Jooste, Y. 2025. Application of the boundary element method for numercial modelling of the seismic hazard at Bambanani gold mine in South Africa. *Journal of the Southern African Institute of Mining and Metallurgy*, vol. 125, no. 11, pp. 661–674

DOI ID:
https://doi.org/10.17159/2411-9717/875/2025

Abstract

This paper presents a novel application of the boundary element method for numerical modelling of the seismic activity and hazard that is associated with the shaft pillar extraction at Bambanani mine in South Africa. In the numerical model, the tabular mining excavations are represented by displacement discontinuity elements, and to accommodate crush, shear, and fault slip seismic events, the numerical model is populated with additional displacement discontinuity elements that represent modelled crush- and shear-type failures in the rockmass. Crush-type failures are evaluated by applying the limit equilibrium method and a Hoek-Brown strength criterion, and shear-type failures are evaluated by applying a Coulomb-friction strength criteria to Ortlepp-shear and geological features. In this paper, the modelling results are presented as time history analyses of modelled potency from 1 January 2010 to 30 June 2022 and normalised exceedance rates for different mining periods using an upper-truncated power law. The normalised exceedance rates of seismic events that have moment magnitude $Mw \geq 1.0$ are lowest for the initial mining period (26 events per year) and highest for the final mining period (218 events per year). The relative errors of the modelled potency and normalised exceedance rates are typically less than 10% or 15%, which suggests that the modelling methodology is appropriate for medium- and longer-term forecasting of seismic activity and hazard, as presented in this paper. Shorter-term forecasting is not considered in this paper.

Keywords

mine seismology, numerical modelling, boundary element method, seismic hazard

Introduction

Seismic activity at underground mines is typically associated with fault slip seismic events that occur on geological features and are similar to crustal earthquakes; shear events that occur on stress-induced shear fractures or shear ruptures, e.g., Ortlepp-shear features at the deep gold mines in South Africa (Van Aswegen, 2008), and crush events that occur as stress fracturing or strain bursting in the rockmass that surrounds the mining excavations (Malovichko, 2020; Van Aswegen, 2021a,b; Malovichko, 2022). From 1 January 2020 to 31 December 2024, the underground seismic systems monitored by the Institute of Mine Seismology (IMS) recorded approximately 1.8 million seismic events that have moment magnitude $-1.0 \leq M_w < 4.0$ at fourteen gold mines in the Witwatersrand Basin (Hanks, Kanamori, 1979; Handley, 2004; Tucker et al., 2016; Frimmel, 2019), including 180,834 events that have $M_w \geq 0.0$, 19,011 events that have $M_w \geq 1.0$, 1,017 events that have $M_w \geq 2.0$ and 17 events that have $M_w \geq 3.0$. The largest seismic event has moment magnitude $M_w = 3.4$ and occurred on 16 March 2020 in the Carletonville gold field and the second and third largest events have $M_w = 3.3$ and occurred on 10 February 2020 and 6 February 2022 in the Carletonville and Klerksdorp gold fields, respectively. Generally, the deep gold mines that extract the tabular orebodies in the Witwatersrand Basin are considered to have significantly higher seismic hazard and therefore higher risk of injuries and fatalities from seismic events than the shallower mines in other regions and countries that have comparably lower seismic hazard and risk. From 1 January 2020 to 31 December 2024, 3,119 injuries and 102 fatalities occurred in the South African gold mining industry (Mthenjane, 2025).

In crustal seismology, prediction of earthquakes is typically described as "extremely difficult" and "effectively impossible" (Kagan, 1997; Geller, 1997) and in mine seismology, short-term forecasting of seismic events using time history analyses is similarly described as "not sufficient" or "not viable" for mitigating the above-mentioned risk of injuries and fatalities Van Aswegen, 2003, 2005; Spottiswoode,

Numerical modelling of the seismic hazard at Bambanani gold mine in South Africa

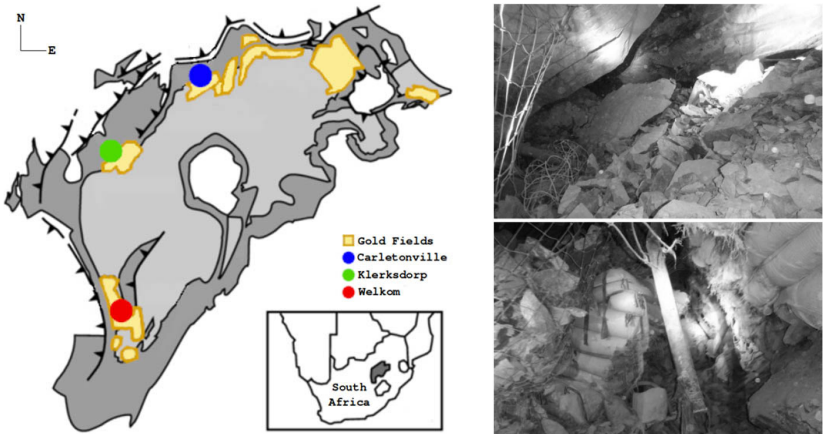

Figure 1—Schematic diagram of the Witwatersrand Basin in South Africa (left) and photographs of underground damage from a seismic event that occurred at Bambanani mine in the Welkom gold field (top and bottom right)

2009, 2010). Until seismic monitoring is considered to have predictive power (Kagan, 1999), numerical modelling applications are probably the primary defenses against the devastations of rockbursts, and therefore Salamon proposed the development of a modelling methodology that accommodates "realistic approximations of the source mechanisms" and facilitates "assessment of the relative hazardousness of various geological environments" (Salamon, 1993; Linkov, 1997, 2002, 2006, 2013; Linkov et al., 2015, 2016). This paper summarises the development of an appropriate and novel modelling methodology for medium- and longer-term forecasting of seismic activity and hazard and presents an application at a South African tabular orebody mine, i.e., the shaft pillar extraction at Bambanani mine in the Welkom gold field (Motsepe et al., 2021; Jooste, 2025). Figure 1 shows a schematic diagram of the Witwatersrand Basin (left) and photographs of underground damage at Bambanani mine (right). The gold fields in the Witwatersrand Basin are shown as yellow regions and the Carletonville, Klerksdorp, and Welkom gold fields are indicated by blue, green, and red dots, respectively (Jolley et al., 2007). The underground photographs correspond to a crush seismic event that has moment magnitude M_w = 1.6 and occurred on 11 October 2021 (Van der Wath et al., 2022).

Seismic monitoring

Source time and location

For a seismic event in this paper, the source time and location are calculated by minimising the travel time residual for the primary and secondary body waves (hereinafter referred to as P- and S-waves, respectively) recorded by a collection of seismic sensors (Salamon, Weibols, 1972; Gibowicz, Kijko, 1994b; Mendecki, Sciocatti, 1997; Mendecki et al., 1999b; Andersen et al., 2002):

$$\psi(t_0, \overline{w_0}) = \sum_{n=0}^{N_{GS}-1} \left|(t_{P,n} - t_0) - \frac{D(\overline{w_0})}{V_{P,n}}\right| + \left|(t_{S,n} - t_0) - \frac{D(\overline{w_0})}{V_{S,n}}\right| \quad [1]$$

where t_0 is the source time of the seismic event, $\overline{w_0} = (w_{0,x}, w_{0,y}, w_{0,z})$ is the source location vector, $\psi(t_0, \overline{w_0})$ is the travel time residual, N_{GS} is the number of seismic sensors, $t_{P,n}$ is the arrival time of the P-wave recorded by the sensor with index $n < N_{GS}$, $t_{S,n}$ is the arrival time of the S-wave, ($t_{B,n}$ - t_0), and ($t_{S,n}$ - t_0) is the travel time of the P- and S-wave respectively, $V_{P,n}$ and $V_{S,n}$ are the corresponding P- and S-wave velocities, and $D(\overline{w_0})$ is the distance from the source location to the sensor. The IMS seismic system at Bambanani mine consists of ten geophone sensors (Bredenkamp et al., 2013), and the average P- and S-wave velocities are approximately V_P = 5300 m/s and V_S = 3550 m/s, respectively.

Source size and scalar potency

In crustal seismology, the source size of a fault slip seismic event is typically expressed using scalar potency or moment, which are calculated by integrating the fault deformation over the slip surface, expressed in Equation 2 (Kanamori, 1977; King, 1978; Ben-Menahem, Singh, 1981; Ben-Zion, Zhu, 2002):

$$P = \iint_{A_0} u(x,y)\delta x \delta y$$
$$M = \frac{\gamma P}{2(1+\nu)} L = \sqrt[3]{\frac{3.5\gamma P}{2(1+\nu)\,\Delta\sigma}} \quad [2]$$

where P is the scalar potency of the fault slip event, $u(x,y)$ is the fault deformation on the slip surface, A_0 is the source area, M is the corresponding scalar moment, L is the average source length, γ is Young's Modulus, ν is Poisson's Ratio, and $\Delta\sigma$ is the average stress drop (Eshelby, 1957). For the Bambanani mine, Young's Modulus is γ = 70GPa, Poisson's Ratio is υ = 0.20, and the average stress drop is $\Delta\sigma$ =1MPa. Figure 2 shows a schematic diagram of a fault slip event. The fault deformation on slip surface is indicated by black arrows, the positive and negative subsurfaces are shown as red and blue regions, respectively, and the source area of the event is shown as a grey region.

In this paper, scalar potency is calculated by constructing the displacement spectra of the P- and S-waves recorded by the IMS seismic system at Bambanani mine (Aki, Richards, 1980; Gibowicz, Kijko, 1994a; Mendecki, Niewiadomski, 1997; Mendecki et al., 1999a):

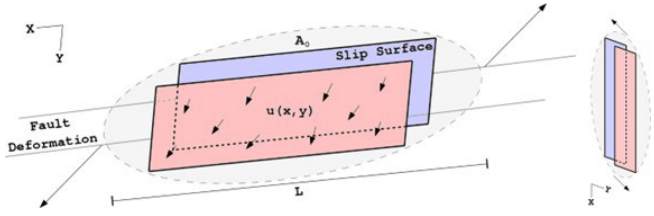

Figure 2—Schematic diagram of a fault slip seismic event. The fault deformation over the slip surface is indicated by black arrows, the subsurfaces are shown as red and blue regions and the source area is shown as a grey region

$$P = 2\pi V_S^2[R_P V_P^3 \Omega_P + R_S V_S^3 \Omega_S] \quad [3]$$

where V_P and V_S are the average P- and S-wave velocities, respectively, $R_P = 0.55$, and $R_S = 0.63$ are the corresponding radiation pattern factors, Ω_P and Ω_S are evaluated by fitting $\Omega(f) = \Omega_P/[1-(f/f_0)^{\gamma\eta}]^{\frac{1}{\gamma}}$ and $\Omega(f) = \Omega_S/[1-(f/f_0)^{\gamma\eta}]^{\frac{1}{\gamma}}$ to the displacement spectra of the P- and S-waves, Ω is the spectral amplitude, f is the spectral frequency, f_0 is the corner frequency, and γ and η are the spectral shape parameters (Brune, 1970; Boatwright, 1980).

Local magnitude and radiated energy

In mine seismology, the combined intensity of a seismic event is sometimes expressed using local magnitude, which is calculated by combining the logarithm of scalar potency as an indicator of the source size and the logarithm of radiated energy as an indicator of the body wave amplitudes (Butler, 1992; Burrows, Ebrahim-Trollope, 2004; Stankiewicz, Essrich, 2004; Mendecki, 2013):

$$m_L = m_P logP + m_E logE + m_0 \quad [4]$$

where m_L is the local magnitude of the seismic event, $logP$ is the logarithm of scalar potency, $logE$ is the logarithm of radiated energy, and m_P, m_E and m_0 are the local magnitude parameters. The local magnitude parameters for Bambanani mine are $m_P = 0.516$, $m_E = 0.344$, and $m_0 = -1.144$ (Butler, Van Aswegen, 1993; Stankiewicz, Essrich, 2004; Ebrahim-Trollope et al., 2013). For a seismic event in this paper, radiated energy and local magnitude are calculated by assuming a simple relationship between the logarithms of scalar potency and radiated energy ($logE = E_P logP + E_0$):

$$E = 10^{E_P logP + E_0}$$
$$m_L = (m_P + m_E E_P) logP + m_E E_0 + m_0 \quad [5]$$

where E is the radiated energy of the seismic event, and E_P and E_0 are the radiated energy parameters. The radiated energy parameters for Bambanani mine are $E_P = 1.0$, and $E_0 = 5.5$. Table 1 summarises the relationship between the logarithms of scalar potency and radiated energy, average source length, moment magnitude ($M_w = 0.667logP + 0.95$), and local magnitude ($m_L = 0.860logP + 0.748$).

Seismic activity and hazard

Seismic activity

In this paper, seismic events supplied by Harmony Gold Mining Company (Jooste, 2023) are considered for different mining periods that are associated with the shaft pillar extraction at Bambanani mine (hereinafter referred to as BAM_10-13, BAM_14-16, BAM_17-19, BAM_20-22, and BAM_ALL). BAM_10-13 spans 1,461 days or 4 years from 1 January 2010 to 31 December 2013 and contains 6207 seismic events that have scalar potency $logP \geq -2.0$ and local magnitude $m_L \geq -1.0$; BAM_14-16 spans 1,096 days or 3 years from 1 January 2014 to 31 December 2016 and contains 13290 seismic events; BAM_17-19 similarly spans 1,095 days from 1 January 2017 to 31 December 2019 and contains 13,714 seismic events; BAM_20-22 spans 943 days or 2.6 years from 1 January 2020 to 30 June 2022 and contains 12,368 seismic events; and BAM_ALL spans 4,595 days or 12.6 years from 1 January 2010 to 30 June 2022.

Figure 3 shows a representative plan of the seismic activity that is associated with the shaft pillar extraction at Bambanani mine. Potentially damaging (PD) seismic events that have scalar potency $logP \geq 0.0$ and local magnitude $m_L \geq 0.7$ are indicated by spheres that are sized by scalar potency and coloured according to the different mining periods such that the blue, green, yellow, and red spheres correspond to BAM_10-13, BAM_14-16, BAM_17-19, and BAM_20-22, respectively. The initial mining excavations of the shaft pillar extraction are shown as grey regions, and the final mining excavations are shown as blue, green, yellow, and red regions that similarly correspond to the mining periods. Some geological features in the rockmass are indicated by black dashed lines.

Figure 4 shows the cumulative number of seismic events recorded by the IMS seismic system at Bambanani mine with respect to calendar time (left) and volume extracted (right) such that the blue, green, yellow, and red lines correspond to BAM_10-13, BAM_14-16, BAM_17-19, and BAM_20-22 respectively. Significantly large (SL) seismic events that have scalar potency $logP \geq 1.0$ and local magnitude $m_L \geq 1.6$ are indicated by circles that are sized by scalar potency and similarly coloured according to the

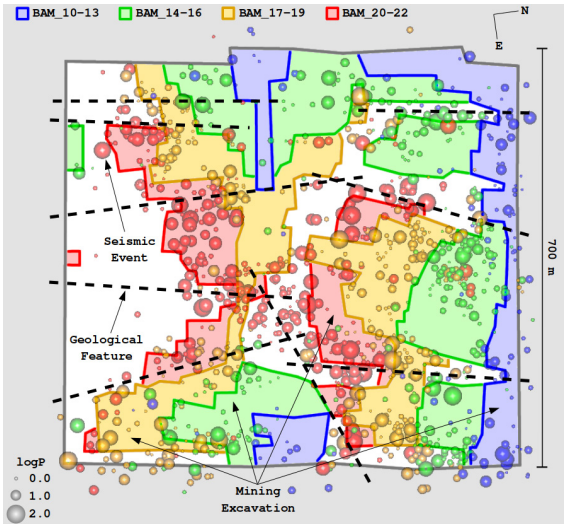

Figure 3—Representative plan of the seismic activity associated with the shaft pillar extraction at Bambanani mine. PD seismic events ($logP \geq 0.0$) are shown as spheres that are sized by scalar potency and coloured blue, green, yellow, and red according to the mining periods. The mining excavations are shown as grey, blue, green, yellow, and red regions. Some geological features in the rockmass are indicated by black dashed lines

Table 1

Relationship between the logarithms of scalar potency and radiated energy, average source length (γ = 70GPa, υ = 0.20, $\Delta\sigma$ = 1MPa), moment magnitude and local magnitude for Bambanani mine

$logP$	-3.0	-2.5	-2.0	-1.5	-1.0	-0.5	0.0	0.5	1.0	1.5	2.0	2.5	3.0	3.5	4.0
$logE$	2.5	3.0	3.5	4.0	4.5	5.0	5.5	6.0	6.5	7.0	7.5	8.0	8.5	9.0	9.5
$L[m]$	5	7	10	15	22	32	47	69	102	149	219	321	472	692	1016
M_w	-1.1	-0.7	-0.4	-0.1	0.3	0.6	1.0	1.3	1.6	2.0	2.3	2.6	3.0	3.3	3.6
m_L	-1.8	-1.4	-1.0	-0.5	-0.1	0.3	0.7	1.2	1.6	2.0	2.5	2.9	3.3	3.8	4.2

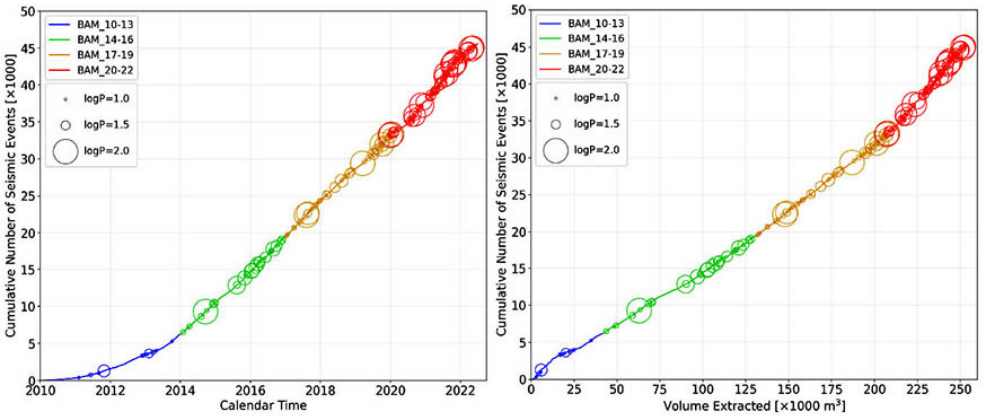

Figure 4—Cumulative number of seismic events with respect to calendar time (left) and volume extracted (right). The blue, green, yellow, and red lines correspond to the different mining periods at Bambanani mine. *SL* seismic events (*logP* ≥ 1.0) are indicated by similarly coloured circles that are sized by scalar potency

different mining periods of the shaft pillar extraction. BAM_10-13 contains 14 SL and 132 PD seismic events; BAM_14-16 contains 39 SL and 326 PD events including the largest event that has $logP$ = 2.3 and m_L = 2.7 and occurred on 19 September 2014; BAM_17-19 contains 60 SL and 379 PD events; and BAM_20-22 contains 97 SL and 392 PD events including the second and third largest events that have $logP$ = 2.2 and m_L = 2.6 and occurred on 22 October 2021 and 22 November 2020, respectively.

Seismic hazard

In mine seismology, seismic hazard is typically expressed as an exceedance probability (Pr), which is calculated by assuming that the source times of seismic events are Poissonian (Kijko, Funk, 1994; Du Toit, Mendecki, 2007) and the source sizes are represented by an upper-truncated power law (Gutenberg, Richter, 1944; Gibowicz, Kijko, 1994c; Burroughs, Tebbens, 2001, 2002; Christensen et al., 2002; Kagan, 2010; Kwiatek et al., 2010; Mendecki, 2012, 2016b):

$$Pr(\geq logQ) = 1 - exp[-N_e(\geq logQ)] \quad [6]$$

where $Pr\ (\geq logQ)$ is the exceedance probability of a seismic event that has scalar potency, $logP \geq logQ$, $logQ$ is the logarithm of scalar potency that corresponds to the exceedance threshold, N_e is the expected number of events that is evaluated by fitting an upper-truncated power law $N_e\ (\geq logQ) = \alpha[10^{-\beta logQ} - 10^{-\beta logP_{max}}]$ to the recorded number of events, P_{max} is the maximum scalar potency of the next record-breaking (RB) seismic event, and α and β are the power-law parameters. In this paper, the maximum scalar potency is estimated using the trend of previous RB seismic events (Chandler, 1952; Robson, Whitlock, 1964; Cooke, 1979; Mendecki, 2016a), and for Bambanani mine, the maximum scalar potency is $logP_{max}$ = 2.5. The power-law parameters are $log\alpha$ = 3.15 and β = 0.765.

Figure 5 shows a comparison of the expected number of seismic events using the upper-truncated power law for BAM_ALL and the number of events recorded by the IMS seismic system at Bambanani mine. The expected number of seismic events that have scalar potency $logP \geq logQ$ is shown as a cyan line, and the recorded number of events that have $logP \geq logQ$ and $logP = logQ$ are, respectively, shown as magenta circles and grey squares that are sized by scalar potency. The number of SL and PD seismic events are appropriately represented by the upper-truncated power law, e.g., the expected number of events are $N_e\ (\geq 1.0)$ = 225 and $N_e\ (\geq 0.0)$ = 1395, respectively, the recorded number of events are $N_r\ (\geq 1.0)$ = 230 and $N_r\ (\geq 0.0)$ = 1357, respectively, and therefore the corresponding relative errors are $|N_e\ (\geq 1.0) - N_r\ (\geq 1.0)|/N_r\ (\geq 1.0)$ = 0.03 and $|N_e\ (\geq 0.0) - N_r\ (\geq 0.0)|/N_r\ (\geq 0.0)$ = 0.02, respectively.

In this paper, seismic hazard is expressed as a simple exceedance rate (Er), which is calculated by scaling the expected number of seismic events using the scalar potency for the different mining periods that are associated with the shaft pillar extraction, i.e., BAM_10-13, BAM_14-16, BAM_17-19, BAM_20-22, and BAM_ALL, and normalising the time span and volume extracted to some reference period:

$$\begin{aligned} Er_T(\geq logQ) &= \frac{T_{ref}}{T_{mp}} N_P(\geq logQ) \\ Er_V(\geq logQ) &= \frac{V_{ref}}{V_{mp}} N_P(\geq logQ) \\ N_P(\geq logQ) &= P_{mp} \frac{N_e(\geq logQ)}{P_{tot}} \\ &= P_{mp} \frac{\alpha}{P_{tot}} [10^{-\beta logQ} - 10^{-\beta logP_{max}}] \end{aligned} \quad [7]$$

where $Er\ (\geq logQ)$ is the exceedance rate of a seismic event that has scalar potency $logP \geq logQ$, T_{mp} and T_{ref} is the time span for the mining period and reference period, respectively, V_{mp} and V_{ref}

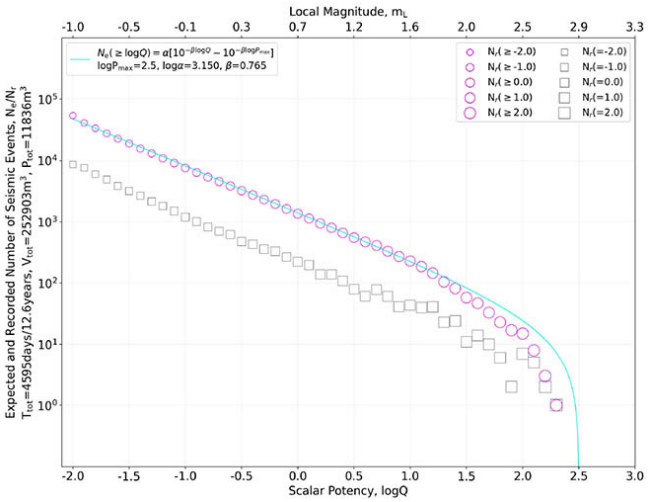

Figure 5—Comparison of the number of seismic events using the upper-truncated power law ($logP_{max}$ = 2.5, $log\alpha$ = 3.15, β = 0.765) and the number of seismic events recorded at Bambanani mine. The expected number of seismic events are shown as a cyan line ($logP \geq logQ$), and the recorded number of events are shown as magenta circles ($logP \geq logQ$) and grey squares ($logP \geq logQ$) that are sized by scalar potency

are the corresponding volume extracted, N_P ($\geq logP$) is the scaled number of seismic events using scalar potency, P_{mp} is the scalar potency for the mining period, and P_{tot} is the total scalar potency of seismic events recorded by the IMS seismic system at Bambanani mine. In this paper, the time span and volume extracted for the reference period is T_{ref} = 60days and V_{ref} = 3300m^3, respectively, and the total scalar potency for BAM_ALL is P_{tot} = 11836m^3. Table 2 summarises the scalar potency of seismic events, time span and volume extracted for the mining periods of the shaft pillar extraction at Bambanani Mine.

Figure 6 shows a comparison of the exceedance rates for the normalised time span (left) and normalised volume extracted (right) such that the blue, green, yellow, red, and black lines correspond to BAM_10-13, BAM_14-16, BAM_17-19, BAM_20-22, and BAM_ALL, respectively. The likelihood of a seismic event that has scalar potency $logP \geq logQ$ (similar to exceedance probability, $Pr = 1 - exp[-Er]$) is indicated by labelled grey regions and described as "unlikely", "possible", "likely", or "probable", i.e., Er_T/Er_V ($\geq logQ$)<0.2 is described as "unlikely", 0.2 ≤ Er_T/Er_V ($\geq logQ$)<2.0 is described as "possible", 2.0 ≤ Er_T/Er_V ($\geq logQ$)<10.0 is described as "likely", and Er_T/Er_V ($\geq logQ$)≥10.0 is described as "probable". The exceedance rates of PD and SL seismic events for the normalised volume extracted are lowest for BAM_10-13 and BAM_14-16, i.e., 8.3 ≤ Er_V (≥0.0) ≤ 12.0 and 1.3 ≤ Er_V (≥1.0)≤1.9, respectively; the exceedance rates are highest for BAM_20-22, i.e., Er_V (≥0.0) = 40.1 and Er_V (≥1.0) = 6.5, respectively; and the exceedance rates for BAM_17-19 are higher than those for BAM_10-13 and BAM_14-16 and lower than those for BAM_20-22, i.e., Er_V (≥0.0) = 17.5 and Er_V (≥1.0) = 2.8, respectively. The exceedance rates for the mining periods of the shaft pillar extraction suggest an increasing trend in the seismic hazard at Bambanani mine, particularly with respect to RB seismic events that have scalar potency $logP \geq 2.3$ and local magnitude $m_L \geq 2.7$ and are described as "unlikely" for the initial mining period and "possible" for the final mining period. The exceedance rates for the normalised time span suggest a similar increasing trend in the seismic hazard.

Numerical modelling

Boundary element method

In the South African gold mining industry, numerical modelling of underground mining excavations is typically performed by applying the Boundary Element Method (BEM) and solving the elasticity equations that correspond to displacement discontinuity (DD) or fictitious force (FF) elements (Salamon, 1964; Starfield, Crouch, 1973; Crouch, 1976a, 1976b; Banerjee, Butterfield, 1981; Crouch, Starfield, 1983; Brebbia, 1984; Napier, Stephansen, 1987; Ryder et al., 1999; Ryder, Malan, 2002). In this paper, the tabular mining excavations at Bambanani mine are approximated using planar surfaces and therefore represented by DD elements in the corresponding BEM model (hereinafter referred to as the DD-BEM model, non-tabular mining excavations are typically represented by FF elements). Figure 7 shows a schematic diagram of a DD element and DD vector $\overline{u} = (u_x, u_y, u_z)$ that represent planar deformation in the local co-ordinate system of the DD surface, i.e., u_x and u_y correspond to shear-type deformation in the XY plane (left and middle, sometimes referred to as ride in the X and Y direction, respectively, similar to fault deformation of a fault slip seismic event), and u_z corresponds to normal-type deformation along the Z axis (right, sometimes referred to as convergence). The planar deformation on the DD surface is indicated by black arrows and the positive and negative subsurfaces with respect to the orientation of the XY plane and Z axis are shown as yellow and green regions, respectively.

Table 2

Scalar potency of seismic events, time span, and volume extracted for the different mining periods that are associated with the shaft pillar extraction at Bambanani mine from 1 January 2010 to 30 June 2022

	BAM_10-13	BAM_14-16	BAM_17-19	BAM_20-22	BAM_ALL
Scalar Potency, P_{mp} [m^3]	880	2748	3438	4770	11836
Time Span, T_{mp} [days/years]	1461/4.0	1096/3.0	1095/3.0	943/2.6	4595/12.6
Volume Extracted, V_{mp} [m^3]	41103	89167	76321	46312	252903

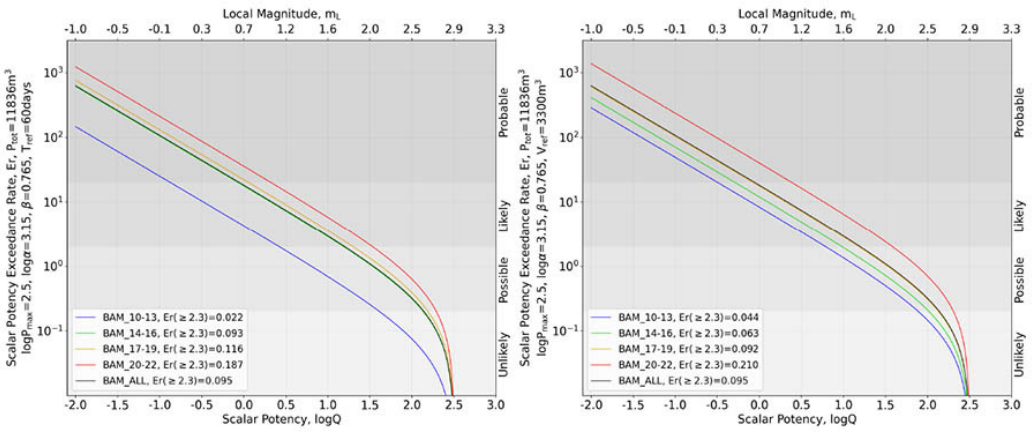

Figure 6—Comparison of the exceedance rates for the normalised time span (left) and normalised volume extracted (right). The blue, green, yellow, and red lines correspond to the mining periods at Bambanani mine. The likelihood of a seismic event that has scalar potency *logP* ≥ *logQ* is indicated by labelled grey regions

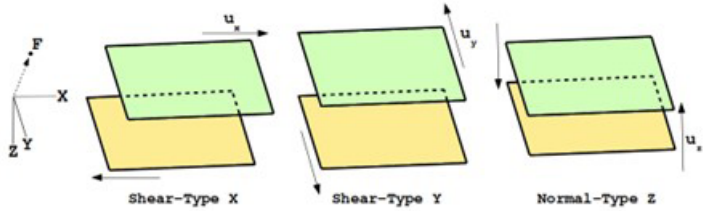

Figure 7—Schematic diagram of a DD element. The DD vector $\overline{u} = (u_x,u_y,u_z)$ represents shear- and normal-type deformation in the XY plane (left and middle) and along the Z axis (right). The planar deformation on the DD surface is indicated by black arrows, and the positive and negative subsurfaces are shown as yellow and green regions

In the DD-BEM model for Bambanani mine, the DD vectors are evaluated by solving the elasticity equations that correspond to a collection of DD elements and satisfy the virgin stress boundary conditions, and the combined stress field is constructed by calculating the induced stress kernels for a collection of points in the rockmass (hereinafter referred to as field points) and combining the induced stress field from the DD elements that represent the mining excavations and the virgin stress field:

$$S_{ij}^k = \begin{bmatrix} S_{xx} & S_{xy} & S_{xz} \\ S_{yx} & S_{yy} & S_{yx} \\ S_{zx} & S_{zy} & S_{zz} \end{bmatrix} = \sum_{k=0}^{N_{DE}-1} \sum \left[S_{ij,x}^{h\to k} u_{h,z} + S_{ij,y}^{h\to k} u_{h,y} + S_{ij,z}^{h\to k} u_{h,z} \right] + p_z^k v_{ij}^k$$

$$v_{ij}^k = \begin{bmatrix} v_{xx} & v_{xy} & v_{xz} \\ v_{yx} & v_{yy} & v_{yx} \\ v_{zx} & v_{zy} & v_{zz} \end{bmatrix} = \begin{bmatrix} 0.013494\,MPa/m & 0.0 & 0.0 \\ 0.0 & 0.013494\,MPa/m & 0.0 \\ 0.0 & 0.0 & 0.026988\,MPa/m \end{bmatrix} \quad [8]$$

where N_{DE} is the number of DD elements, N_{FP} is the number of field points, S_{ij}^k is the combined stress tensor for the field point with index $k < N_{FP}$ in the global co-ordinate system, $S_{ij,x}^{h\to k}$, $S_{ij,x}^{h\to k}$ and $S_{ij,z}^{h\to k}$ are the induced stress kernels for the DD element with index $h < N_{DE}$, $\overline{u}_h = (u_{h,x},u_{h,y},u_{h,z})$ is the corresponding DD vector that satisfies the virgin stress boundary condition $\overline{b}_h = -p_z^h v_{ij} n_h$, p_z^h and n_h are the depth and unit normal vector of the DD element, respectively, v_{ij} is the virgin stress tensor per unit depth and p_z^k is the depth of the field point. For Bambanani mine, the average depth is p_z = 2050m and the virgin stress tensor is $v_{zz} = \rho g = 0.026988\ MPa/m$ and $v_{xx} = v_{yy} = v_{zz}/2 = 0.013494\ MPa/m$, where $\rho = 2750k\ g/m^3$ is the density of the rockmass and g = 9.81 m/s² is gravitational acceleration. The normal- and shear-type stress for a field point that is associated with a planar surface in the DD-BEM model is calculated by transforming the combined stress tensor to a traction vector:

$$S_{nt}^k = \overline{S_{ct}^k} \cdot n_k \overline{S_{ct}^k} = S_{ij}^k n_k$$
$$S_{st}^k = \left| \overline{S_{ct}^k} - \left(\overline{S_{ct}} \cdot n_k \right) n_k \right| \quad [9]$$

where S_{nt}^k and S_{st}^k is the normal- and shear-type stress, respectively, $\overline{S_{ct}^k} = S_{ij}^k n_k$ is the combined traction vector for the field point with index $k < N_{FP}$, and n_k is the unit normal vector for the planar surface.

Modelled crush- and shear-type failures

Modelled crush-type failures

To accommodate crush seismic events at Bambanani mine, the DD-BEM model is populated with field points and additional DD elements that are constructed from the tabular orebody that surrounds the mining excavations and represent modelled crush-type failures in the rockmass. In this paper, the tabular orebody is approximated using planar surfaces (similar to tabular mining excavations) and the corresponding crush-type field points are evaluated using an excess normal stress (ENS) threshold, which is calculated by applying the limit equilibrium method (LEM) and a peak Hoek-Brown strength criterion (Hoek, Brown, 1980; Barron, 1984; Barron, Pen, 1992; Hoek, Marinos, 2007; Napier, Malan, 2007, 2011, 2012; Ilchev, 2013a, 2013b; Napier, Malan, 2014, 2018, 2021):

$$ENS = S_{nt}^k - \tau_{n0}$$
$$\tau_{n0} = S_{le} + \tau_{c0} \left[\frac{r_0}{\tau_{c0}} S_{le} + q_0 \right]^{\frac{1}{2}} \quad [10]$$

where τ_{n0} is the peak normal-type strength, S_{nt}^k is the normal-type stress for the crush-type field point and additional DD element with index $k < N_{FP}$, τ_{c0} is the peak uniaxial compressive strength of the rockmass, r_0 and q_0 are the peak Hoek-Brown strength parameters, and S_{le} is the transverse-type stress from the LEM. For a crush-type field point that exceeds the ENS threshold and therefore has $ENS > 0$, the boundary condition of the additional DD element is modified to accommodate the residual strength of the modelled crush-type failure and the corresponding crush-type deformation in the DD-BEM model for Bambanani mine (similar to convergence of mining excavations):

$$\overline{b}_k = -p_z^k v_{ij} n_k + \tau_{n1} n_k$$
$$\tau_{n1} = S_{le} + \tau_{c1} \left[\frac{r_1}{\tau_{c1}} S_{le} + q_1 \right]^{\frac{1}{2}} \quad [11]$$

where τ_{n1} is the residual normal-type strength, τ_{c1} is the residual uniaxial compressive strength, and r_1 and q_1 are the residual Hoek-Brown strength parameters. The DD vectors of the additional DD elements are iteratively evaluated by solving the elasticity equations that satisfy the residual strength boundary conditions until all crush-type field points have $ENS \le 0$. For the crush-type field points in the paper, the peak and residual uniaxial compressive strength of the rockmass is τ_{c0} = 200MPa and τ_{c1} = 20MPa, respectively, the peak Hoek-Brown strength parameters are r_0 = 4.0 and q_0 = 0.02, and the residual Hoek-Brown strength parameters r_1 = 1.5 and q_1 = 0.02 (Ryder, Jager, 2002).

Modelled shear-type failures

To accommodate shear and fault slip seismic events, the DD-BEM model for Bambanani mine is similarly populated with field points and additional DD elements that represent modelled shear-type failures in the rockmass and are evaluated using excess shear stress (ESS) thresholds, which are calculated by applying a simple Coulomb-friction strength criteria (Ryder, 1987; Napier, 1987; Spottiswoode, 1988; Ryder, 1988; Jager, Ryder, 1999a; Ryder et al., 2002):

$$ESS = S_{st}^k - \tau_{s0} \text{ or } S_{st}^k - \tau_{s1}$$
$$\tau_{s0} = S_{nt}^k tan\phi_0 + C_0$$
$$\tau_{s1} = S_{nt}^k tan\phi_1 + C_1 \quad [12]$$

where τ_{s0} is the peak shear-type strength for the peak ESS threshold, τ_{s1} is the residual shear-type strength for the residual ESS threshold, S_{st}^k is the shear-type stress for the shear-type field point and additional DD element with index $k < N_{FP}$, S_{nt}^k is the corresponding normal-type stress, ϕ_0 and C_0 are the peak friction angle and peak cohesion, respectively, and ϕ_1 and C_1 are the residual friction angle and residual cohesion, respectively. In this paper, the shear-type field points are constructed from the planar surfaces of Ortlepp-shear features that surround the mining excavations and correspond to the orientation of maximum ESS (Gay, Ortlepp, 1979; Ortlepp et al., 1997; Ortlepp, 2000; Ortlepp et al., 2005; Van Aswegen, Stander, 2012; Van Aswegen, 2013) and geological features that are approximated using additional planar surfaces that correspond to the digitised faults supplied by Harmony Gold Mining Company. For Ortlepp-shear features in this paper, the peak and residual friction angle is $\phi_0 = \phi_1 = 30°$ and the peak and residual cohesion is $C_{0c} = 20$MPa and $C_1 = 0$MPa, respectively, and for geological features in the rockmass, the peak friction angle is $\phi_0 = 25°$, the residual friction angle is $\phi_1 = 20°$, and the peak and residual cohesion is $C_0 = 10MPa$ and $C_1 = 0MPa$, respectively (Bieniawski, 1967; Byerlee, 1978; Jager, Ryder, 1999b; Ryder, 2002 James et al., 2007; Hofmann, Scheepers, 2011; Hofmann et al., 2013; Van Aswegen, 2020; Hofmann, 2024).

For a shear-type field point or modelled shear-type failure that exceeds the *ESS* thresholds in the DD-BEM model and therefore has peak *ESS* > 0 or residual ESS > 0, the DD vector of the additional DD element is iteratively modified to accommodate the corresponding shear-type deformation (similar to ride of mining excavations) until all shear-type field points have peak *ESS* ≤ 0 and all shear-type failures have residual *ESS* ≤ 0. Figure 8 shows the modelled shear-type failures that are associated with the different mining periods of the shaft pillar extraction at Bambanani mine, i.e., BAM_10-13, BAM_14-16, BAM_17-19, and BAM_20-22 (from top left to bottom right). The black-to-white contours indicate the cumulative shear-type deformation on the DD surfaces of the additional DD elements that represent the Ortlepp-shear and geological features in the DD-BEM model. The initial mining excavations are shown as grey regions and the final mining excavations are shown as blue, green, yellow, and red regions that correspond to BAM_10-13, BAM_14-16, BAM_17-19, and BAM_20-22, respectively.

Modelled potency and hazard

In the DD-BEM model for Bambanani mine, the planar size of a modelled crush- or shear-type failure is expressed using modelled potency, which is calculated by integrating the planar deformation over the DD surface of the additional DD element (similar to scalar potency of a fault slip seismic event):

$$P_k' = \iint_{A_k} [|\overline{u_k}(x,y) \cdot n_k| + |\overline{u_k}(x,y) - [\overline{u_k}(x,y) \cdot n_k] n_k|] \, \delta x \delta y = [|\overline{u_k} \cdot n_k| + |\overline{u_k} - [\overline{u_k} \cdot n_k] n_k|] A_k \quad [13]$$

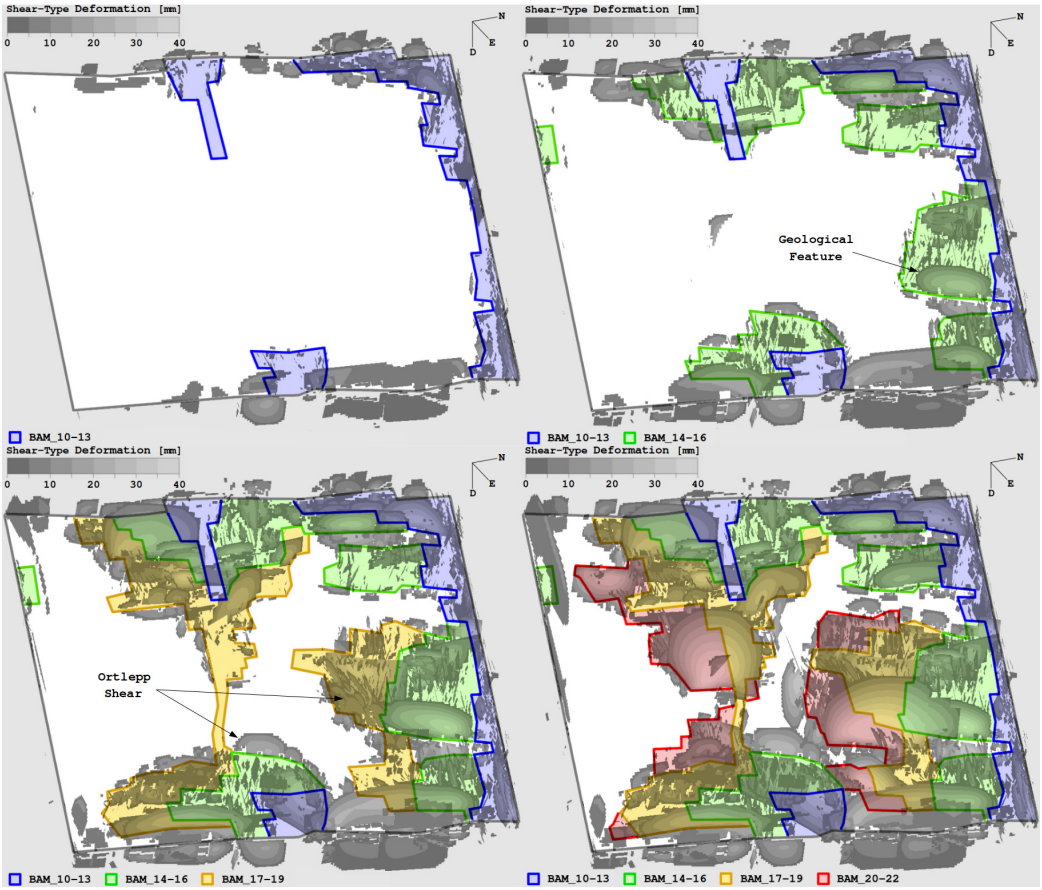

Figure 8—Modelled shear-type failures for the different mining periods of the shaft pillar extraction at Bambanani mine (from top left to bottom right). The cumulative shear-type deformation on the DD surfaces that represent shear-type failures is indicated by black-to-white contours. The initial mining excavations are shown as grey regions, and the final mining excavations are shown as blue, green, yellow, and red regions

where P'_k is the modelled potency of the additional DD element with index $k < N_{FP}$ that represents a modelled crush- or shear-type failure in the DD-BEM model, $\overline{u_k}(x,y) = \overline{u_k} = (u_{k,x}, u_{k,y}, u_{k,z})$ is the corresponding DD vector, n_k is the unit normal vector, and A_k is the planar area of the DD surface.

In this paper, the modelled hazard is expressed as an exceedance rate (Er'), which is calculated by scaling the expected number of seismic events using the modelled potency of the crush- and shear-type failures that exceed the ENS and ESS thresholds in the DD-BEM model for Bambanani mine and normalising the time span and volume extracted for the different mining periods of the shaft pillar extraction to some reference period (similar to the seismic hazard using scalar potency):

$$Er'_T(\geq logQ) = \frac{T_{ref}}{T_{mp}} N'_P(\geq logQ)\ Er'_V(\geq logQ) = \frac{V_{ref}}{V_{mp}} N'_P(\geq logQ)$$
$$N'_P(\geq logQ) = P'_{mp} \frac{N_e(\geq logQ)}{P_{tot}} = P'_{mp} \frac{\alpha}{P_{tot}} [10^{-\beta logP} - 10^{-\beta logP_{max}}] \quad [14]$$
$$P'_{mp} = \sum_{k=0}^{N_{FP}-1} [max(P'_{k+} - P'_{k-}, 0)]$$

where Er' ($\geq logQ$) is the exceedance rate of a seismic event that has scalar potency $logP \geq logQ$, T_{mp} is the time span for the mining period, T_{ref} = 60 days is the time span for the reference period, V_{mp} and V_{ref} = 3300m^3 are the corresponding volume extracted for the mining period and reference period, respectively, $N'_P(\geq logQ)$ is the scaled number of seismic events using the modelled potency of the crush- and shear-type failures, $N_e(\geq logQ) = \alpha[10^{-\beta logQ} - 10^{-\beta logP_{max}}]$ is the expected number of seismic events using the upper-truncated power law, P_{tot} = 11836 m^3 is the total scalar potency, P_{max} = 2.5 is the maximum scalar potency of the next RB seismic event, $log\alpha$ = 3.15 and β = 0.765 are the power-law parameters, P'_{mp} is the modelled potency for the mining period, N_{FP} is the number of field points, P'_{k+} is the final modelled potency of a crush- or shear-type failure that corresponds to the additional DD element with index $k < N_{FP}$, and P'_{k-} is the initial modelled potency.

Modelling results

In the DD-BEM model for Bambanani mine, the tabular mining excavations are subdivided according to a collection of digitised mining steps supplied by Harmony Gold Mining Company (Van Der Wath, 2023); the modelled potency of the crush- and shear-type failures is calculated for the corresponding mining steps; and the modelled hazard is calculated for the different mining periods that are associated with the shaft pillar extraction, i.e., BAM_10-13, BAM_14-16, BAM_17-19, BAM_20-22, and BAM_ALL. The DD-BEM model has 150 subdivided mining steps that correspond to the calendar months from 1 January 2010 to 30 June 2022, i.e., BAM_10-13 contains 48 mining steps that correspond to the calendar months from 1 January 2010 to 31 December 2013; BAM_14-16 and BAM_16-19 contain 36 mining steps from 1 January 2014 to 31 December 2016 and from 1 January 2017 to 31 December 2019, respectively; and BAM_19-22 contains 30 mining steps from 1 January 2020 to 30 June 2022. The tabular mining excavations at Bambanani mine typically strike northwards, dip eastwards at approximately 20° and are represented by 250 thousand DD elements that have 1 × 1 m, 2 × 2 m, 4 × 4 m, and 8 m × 8 m dimensions. To accommodate modelled crush-type failures, the tabular orebody that surrounds the mining excavations is represented by an additional 150 thousand DD elements that have 2 m × 2 m dimensions, and to accommodate modelled shear-type failures, the Ortlepp-shear and geological features are represented by an additional 400,000 DD elements that have 4 m × 4 m dimensions. The faults at Bambanani mine typically strike southwards and dip westwards at approximately 70°.

Figure 9 shows a comparison of the cumulative modelled potency and cumulative scalar potency with respect to calendar time (left) and volume extracted (right) such that the blue, green, yellow, and red lines correspond to BAM_10-13, BAM_14-16, BAM_17-19, and BAM_20-22, respectively. The solid lines indicate the cumulative modelled potency of the additional DD elements that represent modelled crush- and shear-type failures in the DD-BEM model, and the dashed lines indicate the cumulative scalar potency of seismic events recorded by the IMS seismic system at Bambanani mine. Table 3 summarises the modelled potency, scalar potency, time span, and volume extracted for the mining periods that are associated with the shaft pillar extraction. Figure 10 shows a comparison of the modelled potency and scalar potency exceedance rates for the normalised time span (left) and normalised volume extracted (right) such that the blue, green, yellow, red, and black lines correspond to BAM_10-13, BAM_14-16, BAM_17-19, BAM_20-22, and BAM_ALL, respectively. The solid lines indicate the exceedance rates using the modelled potency of the crush- and shear-type failures that exceed the ENS and ESS thresholds in the DD-BEM model for Bambanani mine, and the dashed lines indicate

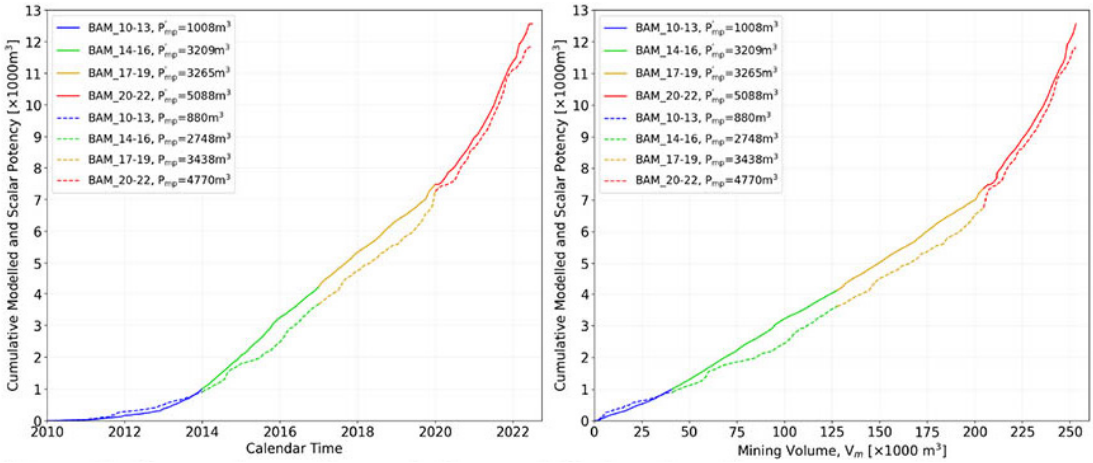

Figure 9—Comparison of cumulative modelled and scalar potency with respect to calendar months (left) and volume extracted (right). The solid lines indicate cumulative modelled potency, the dashed lines indicate cumulative scalar potency, and the lines are coloured according to the different mining periods at Bambanani mine

Table 3

Modelled potency, scalar potency, time span and volume extracted for the different mining periods associated with the shaft pillar extraction at Bambanani mine from 1 January 2010 to 30 June 2022

	BAM_10-13	BAM_14-16	BAM_17-19	BAM_20-22	BAM_ALL
Modelled Potency, P'_{mp} [m^3]	1008	3209	3265	5088	12570
Scalar Potency, P_{mp} [m^3]	880	2748	3438	4770	11836
Time Span, T_{mp} [days/years]	1461/4.0	1096/3.0	1095/3.0	943/2.6	4595/12.6
Volume Extracted, V_{mp} [m^3]	41103	89167	76321	46312	252903

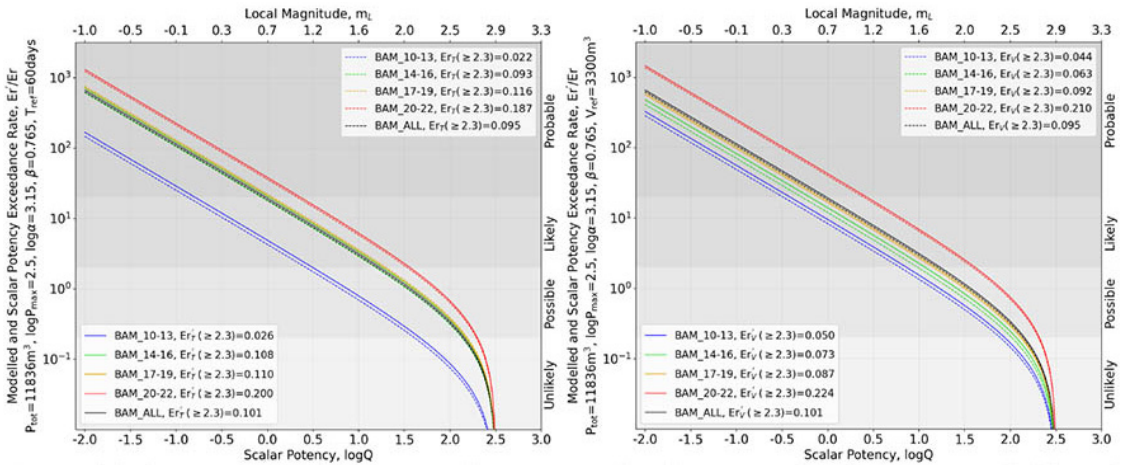

Figure 10—Comparison of the exceedance rates for the normalised time span (left) and normalised volume extracted (right). The solid and dashed lines indicate the exceedance rates using modelled potency and scalar potency, respectively. The lines are coloured according to the mining periods at Bambanani mine

the corresponding exceedance rates using the scalar potency of seismic events. The likelihood of a seismic event that has scalar potency $logP \geq logQ$, is indicated by labelled grey regions and described as "unlikely", "possible", "likely" or "probable", e.g., $0.2 \leq Er'_T/Er'_V\ (\geq logQ) < 2.0$ is described as "possible", and $Er'_T/Er'_V\ (\geq logQ) \geq 10.0$ is described as "probable".

The modelled hazard is a reasonably accurate estimation of the seismic hazard for the different mining periods of the shaft pillar extraction at Bamabanani mine. The modelled potency of the crush- and shear-type failures overestimates the scalar potency of seismic events for BAM-10-13, BAM_14-16, and BAM_20-22, i.e., the modelled potency is P'_{mp} = 1008m^3, 3209m^3, and 5088m^3, respectively; the scalar potency is P'_{mp} = 880m^3, 2748m^3, and 4770m^3, respectively; and the relative error is $[P'_{mp} - P_{mp}]/P'_{mp} = 0.12$, 0.14, and 0.06, respectively. The modelled potency underestimates the scalar potency for BAM_17-19, i.e., the modelled potency is P'_{mp} = 3265m^3, the scalar potency is P_{mp} = 3438m^3, and the relative error $[P'_{mp} - P_{mp}]/P'_{mp} = -0.05$. The modelled potency exceedance rates similarly overestimate and underestimate the scalar potency exceedance rates. The modelled potency exceedance rates of PD and SL seismic events are lowest for BAM_10-13, i.e., Er'_V (≥0.0) = 9.5 and Er'_V (≥1.0) = 1.5, respectively; the exceedance rates are highest for BAM_20-22, i.e., Er'_V (≥0.0) = 42.8 and Er'_V (≥1.0) = 6.9, respectively; and the exceedance rates for BAM_14-16 and BAM_17-19 are higher than those for BAM_10-13 and lower than those for BAM_20-22, i.e., $14.0 \leq Er'_V$ (≥0.0) ≤16.6 and $2.3 \leq Er'_V$ (≥1.0)≤2.7, respectively.

In the DD-BEM model for Bambanani mine, the spatial intensity of the modelled potency is expressed as a planar density, which is calculated by radially filtering the modelled crush- and shear-type failures that exceed the ENS and ESS thresholds according to a collection of grid points:

$$P^{l\prime}_{gd} = \sum_{k=0}^{N_{FP}-1} \chi(\overline{w_k})[max(P'_{k+} - P'_{k\text{-}}, 0)]$$

$$\chi(\overline{w_k}) = \left\{ \begin{matrix} 0 D(\overline{w_k}) > R \\ \frac{1}{\pi R^2} D(\overline{w_k}) \leq R \end{matrix} \right\} R = 100m \quad [15]$$

where N_{GP} is the number of grid points, $P^{l\prime}_{gp}$ is the planar density of the modelled potency for the grid point with index $l < N_{GP}$, N_{FP} is the number of field points, P'_{k+} is the final modelled potency of the additional DD element with index $k < N_{FP}$ that represents a modelled crush- or shear-type failure in the DD-BEM model, $P'_{k\text{-}}$ is the initial modelled potency, $\overline{w_k} = (w_{k,x}, w_{k,y}, w_{k,z})$ is the corresponding DD location vector, $\chi(\overline{w_k})$ is the gridding factor, $D(\overline{w_k})$ is the distance from the additional DD element to the grid point, and R = 100 m is the gridding radius. The spatial intensity of the scalar potency is similarly calculated by radially filtering seismic events recorded by the IMS seismic system at Bambanani Mine:

$$P^{l}_{gp} = \sum_{n=0}^{N_{SE}-1} \chi(\overline{w_n}) P_n \quad [16]$$

where P^{l}_{gp} is the planar density of the scalar potency, N_{SE} is the number of seismic events, P_n is the scalar potency of the seismic event with index $n < N_{SE}$ and $\overline{w_n} = (w_{n,x}, w_{n,y}, w_{n,z})$ is the corresponding source location vector. Figure 11 shows the planar density of the modelled potency (left) and scalar potency (right) at Bambanani mine. The black-to-white contours indicate the planar density, and the "hotspots" in the spatial intensity that have planar density $(P^{l\prime}_{gp}/P^{l}_{gp} \geq 0.3)$ are shown as cyan and magenta regions. Some geological features are indicated by black dashed lines.

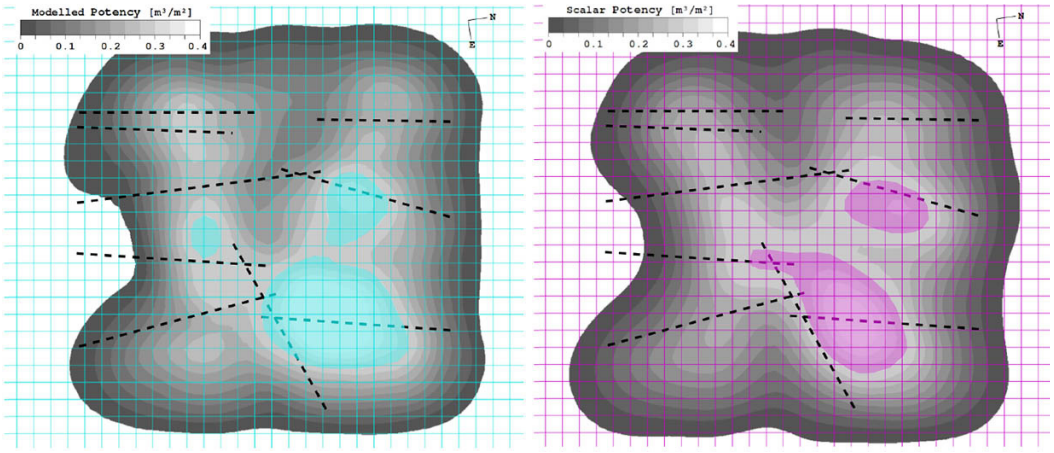

Figure 11—Planar density of the modelled potency (left) and scalar potency (right) at Bambanani mine. The planar density is indicated by black-to-white contours and the "hotspots" in the spatial intensity ($P_{gp}^{l\prime}/P_{gp}^{l} \geq 0.3$) are shown as cyan and magenta regions. Some geological features are indicated by black dashed lines

Comments

In this paper, the modelled potency and modelled hazard are presented for medium- and longer-term mining periods that are associated with the shaft pillar extraction at Bambanani mine, i.e., BAM_10-13, BAM_14-16, BAM_17-19, BAM_20-22, and BAM_ALL, and the modelling results suggest an increasing trend in the modelled hazard that is a reasonably accurate estimation of the seismic hazard. The modelled potency exceedance rates of RB seismic events for BAM_10-13, BAM_14-16, BAM_17-19, BAM_20-22, and BAM_ALL are Er_V' (≥2.3) = 0.050, 0.073, 0.087, 0.224, and 0.101, respectively, and the scalar potency exceedance rates are Er_V' (≥2.3) = 0.044, 0.063, 0.092, 0.210, and 0.095, respectively. The relative error is typically lower than 10% or 15%, e.g., $[Er_V' - Er_V]/Er_V'$ = 0.12, 0.14, -0.05, 0.06 and 0.06, respectively. The relative errors for shorter term mining periods are probably higher and not considered in this paper. The "hotspots" in the spatial intensity of the modelled potency are similar to those of the scalar potency. Generally, the modelling results suggest that the modelling methodology is appropriate for medium- and longer term forecasting of seismic activity and hazard, particularly for the comparison of different mining periods as presented in this paper. The modelling methodology is probably not appropriate for shorter term forecasting or prediction of seismic events.

References

Aki, K., Richards, P.G. 1980. Quantitative Seismology. Theory and Methods. W.H. Freeman and Company, San Francisco.

Andersen, L.M., Ryder, J.A., Goldbach, O.D. 2002. A Textbook on Rock Mechanics for Tabular Hard Rock Mines, chapter 5.3, seismology, location of seismic events, pp. 204–210.

Banerjee, P.K., Butterfield, R. Boundary element methods in engineering science. McGraw & Hill, 1981.

Barron, K. 1984. Analytical approach to the design of coal pillars. *CIM Bulletin,* vol. 77, no. 868, pp. 37–44. .

Barron, K., Pen, Y. 1992. A revised model for coal pillars. In *Proceedings of the Workshop on Coal Pillar Mechanics and Design*, vol. 9315, p. 144. United States, Department of the Interior, Bureau of Mines.

Ben-Menahem, A., Singh, S.J. 1981. Seismic Waves and Sources. Springer-Verlag, New York.

Ben-Zion, Y., Zhu, L. 2002. Potency-magnitude scaling relation for southern California earthquakes with 1.0<M<7.0. *Geophysical Journal International,* vol. 148, pp. F1–F5.

Bieniawski, Z.T. 1967. Mechanism of brittle fracture of rock: part 1 theory of the fracture process. In *International Journal of Rock Mechanics and Mining Sciences & Geomechanics Abstracts*, vol. 4, pp. 395–406. Elsevier.

Boatwright. J. 1980. A spectral theory for circular seismic sources; simple estimates of source dimension, dynamic stress drop, and radiated seismic energy. B*ulletin of the Seismological Society of America*, vol. 70, no. 1, pp. 1–27.

Brebbia, C.A. 1984. The Boundary Element Method for Engineers. 97807273020. Pentech Press, ISBN 0727302051

Bredenkamp, A.F.L., Goldswain, G., Green, M. 2013. 4.5Hz Geophone Sensors. Technical report, *Institute of Mine Seismology*.

Brune, J.N. 1970. Tectonic stress and the spectra of seismic shear waves from earthquakes. *Journal of Geophysical Research*, vol. 75, no. 26, pp. 4997–5009.

Burroughs, SM, Tebbens, S.F. 2002. The upper-truncated power law applied to earthquake cumulative frequency-magnitude distributions: Evidence for a time-independent scaling parameter. *Bulletin of the Seismological Society of America*, vol. 92, no. 8, pp. 2983–2993.

Burroughs, S.M., Tebbens, S.F. 2001. Upper-truncated power law distributions. *Fractals*, vol. 9, no. 02, pp. 209–222.

Burrows, D., Ebrahim-Trollope, R. 2004. Seismic magnitude and its application in the industry. In *SANIRE Symposium Proc, The Miners Guide Through the Earths Crust*,(J) Lass eds.), Potchefstroom, South Africa.

Butler, A.G. 1992. Magnitude evaluation for mining regions using the integrated seismic system. Technical report, ISS International.

Butler, A.G., van Aswegen, G. 1993. Ground velocity relationship based on a large sample of underground measurement in two south african mining regions. *Proceedings of the 3rd International Symposium on Rockbursts and Seismicity in Mines.*

Byerlee, J. 1978. Friction of rocks. Rock friction and earthquake prediction, pp. 615–626.

Cooke, P. 1979. Statistical inference for bounds of random variables. Biometrika, vol. 66, no. 2, pp. 367–374.

Christensen, K., Danon, L., Scanlon, T., Bak, P. 2002. Unified scaling law for earthquakes. *Proceedings of the National Academy of Sciences*, vol. 99(suppl_1), pp. 2509–2513.

Crouch, S.L. 1976a. nalysis of stress and displacements around underground excavations: an application of the displacement discontinuity method. Technical report, Department of Civil and Mineral Engineering, University of Minnesota.

Crouch, S.L. 1976b. Solution of plane elasticity problems by the displacement discontinuity method. *International Journal of Numerical Methods in Engineering*, vol. 10, pp. 301–343.

Crouch, S.L., Starfield, A.M. 1983. Boundary Element Methods in Solid Mechanics: With Applications in Rock Mechanics and Geological Engineering. Allen & Unwin, 1983. ISBN 004620010X, 9780046200107.

Dennison, R.J.G., van Aswegen, G. 1993. Stress Modelling and Seismicity on the Tanton Fault: A Case Study in a South African Gold Mine. In *Proceedings of the 3rd International Symposium on Rockbursts and Seismicity in Mines*, p. 327, Kingston, Ontario, Canada.

Dor, O., Reches, Z., van Aswegen, G. 2001. Fault zones associated with the matjhabeng earthquake, 1999, South Africa. In *5th International Symposium on Rockbursts and Seismicity in mines*, pp. 109–112.

Du Toit, C., Mendecki, A.J. 2007. Examples of time distribution of seismic events in mines. In IUGG Conference, Session on Induced Seismicity (SW006), Perugia.

Ebrahim-Trollope, R., Durrheim, R.J., Smith, G. 2013. Measuring the size of mining-induced earthquakes: a proposal. In *13th SAGA Biennial Conference and Exhibition*. European Association of Geoscientists & Engineers, pp. cp–378.

Eshelby, J.D. 1957. The determination of the elastic field of an ellipsoidal inclusion and related problems. *Proceedings of the Royal Society of London*, Series A, Mathematical and Physical Sciences, 241(1226):376–396, August 1957.

Frimmel, H.E. 2019. The witwatersrand basin and its gold deposits. The Archaean geology of the Kaapvaal craton, southern Africa, pp. 255–275.

Gay, N.C. Ortlepp, W.D. 1979. Anatomy of a mining-induced fault zone. *Geological Society of America Bulletin*, vol. 90, no. 1, pp. 47–58.

Geller, R.J. 1997. Earthquake prediction: a critical review. *Geophysical Journal International*, vol. 131, no. 3, pp. 425–450.

Gibowicz, S.J., Kijko, A. 1994a. An Introduction to Mining Seismology, chapter 11, seismic spectra and source parameters, pages 264–300.

Gibowicz, S.J., Kijko, A. 1994b. An Introduction to Mining Seismology, chapter 4, location of seismic events in mines , pages 48–77.

Gibowicz, S.J., Kijko, A. 1994c. An Introduction to Mining Seismology, chapter 12.3, Statistical Assessment of Seismic Hazard in Mines: Statistical Prediction, The Gutenberg-Richter Frequency-Magnitude Distribution, pp. 301–310.

Gutenberg, B., Richter, C.F. 1944. Frequency of earthquakes in california. *Bulletin of the Seismological Society of America*, vol. 34, no. 4, pp. 185–188.

Handley, J.R.F. 2004. Historic overview of the Witwatersrand Goldfields: A review of the discovery, geology, geophysics, development, mining, production and future of the Witwatersrand Goldfields as seen through a geological and financial association spanning 50 years.

Hanks, T.C. Kanamori, H. 1979. A moment magnitude scale. *Journal of Geophysical Research*, vol. 84, pp. 2348–2350.

Hoek, E., Brown, E. 1980. Empirical strength criterion for rock masses. *Journal of the Geotechnical Engineering Division*, ASCE, 106, 09. doi: 10.1061/AJGEB6.0001029

Hoek, E., Marinos, P. 2007. A brief history of the development of the hoek-brown failure criterion[j]. *Soils and Rocks*, 30, 05. doi: 10.28927/SR.302085

Hofmann, G., Scheepers, L. 2011. Simulating fault slip areas of mining induced seismic tremors using static boundary element numerical modelling. *Mining Technology*, vol. 120, pp. 53–64, 03 doi: 10.1179/037178411X12942393517291

Hofmann, G.F., Scheepers, L., Ogasawara, H. 2013. Loading conditions of geological faults in deep level tabular mines. In P*roc. 6th Int. Symp. In-Situ Rock Stress*. Sendai: Tohoku University, pp. 560–580.

Hofmann, G.F. 2024. Excess shear stress analysis of complex geological structures in underground mines. In *Deep Mining 2024: Proceedings of the 10th International Conference on Deep and High Stress Mining*, Australian Centre for Geomechanics. pp. 673–686.

Ilchev. A. 2013a. Comments on the implementation of the limit equilibrium method. Technical report. *Institute of Mine Seismology*.

Ilchev. A. 2013b. The limit equilibrium conjecture. Technical report, *Institute of Mine Seismology*.

Jager, A.J., Ryder, J.A. 1999a. A Handbook on Rock Engineering Practice for Tabular Hard Rock Mines, chapter 3.2.3, stoping layouts, excess shear stress, pp. 51–53.

Jager, A.J., Ryder, J.A. 1999b. A Handbook on Rock Engineering Practice for Tabular Hard Rock Mines, chapter 1.3.2, rock strength and friction properties, pages 13–14.

James, J.V., Rangasamy, T., Petho, S.P. 2007. Excess shear stress analysis of seimicity associated with dykes. In *Deep Mining 2007: Proceedings of the Fourth International Seminar on Deep and High Stress Mining*, pp. 21–30. Australian Centre for Geomechanics.

Jolley, S., Stuart, G., Freeman, S., Knipe, R., Kershaw, D., McAllister, E. 2007. Andrew Barnicoat, and R. Tucker. Progressive evolution of a late orogenic thrust system, from duplex development to extensional reactivation and disruption: Witwatersrand basin, south africa. *Geological Society*, London, Special Publications, 272:543–569, 05 2007. doi: 10.1144/GSL.SP.2007.272.01.28

Jooste. Y. 2025. A Numerical Modelling Methodology for Deep-Level Tabular Excavations using a Combined Bulking and Limit Equilibrium Constitutive Model, chapter 6, Monitoring during the Shaft Pillar Extraction at Bambanani Mine. PhD thesis, University of Pretoria.

Jooste. Y. 2023. Seismic events associated with the shaft pillar extraction at bambanani mine, supplied by harmony gold.

Kagan, Y.Y. 1997. Are earthquakes predictable? *Geophysical Journal International*, vol. 131, no. 3. pp. 505–525. https://academic.oup.com/gji/article/131/3/505/2140303

Kagan, Y.Y. 1999. Is earthquake seismology a hard, quantitative science? Seismicity Patterns, Their Statistical Significance and Physical Meaning, pp. 233–258.

Kagan, Y. 2010. Earthquake size distribution: Power-law with exponent 0.5? *Tectonophysics*, vol. 490, no. 1-2, pp. 103–114.

Kanamori, H. 1977. The energy release in great earthquakes. *Journal of Geophysical Research*, vol. 82, no. 20, pp. 2981–2987.

KN53463 Chandler. 1952. The distribution and frequency of record values. *Journal of the Royal Statistical Society: Series B* (Methodological), vol. 14, no. 2, pp. 220–228.

Kijko, A., Funk, C.W. 1994. The assessment of seismic hazards in mines. *Journal of the Southern African Institute of Mining and Metallurgy*, vol. 94, no. 7, pp. 179–185.

King, G.C.P. 1978. Geological faults, fractures, creep and strain. *Philosophical Transactions of the Royal Society of London. Series A, Mathematical and Physical Sciences*, 288(1350), pp. 197–212, February.

Kwiatek, G., Plenkers, K., Nakatani, M., Yabe, Y., Dresen, G., JAGUARS-Group. 2010. Frequency-magnitude characteristics down to magnitude-4.4 for induced seismicity recorded at mponeng gold mine, south africa. *Bulletin of the Seismological Society of America*, vol. 100, no. 3, pp. 1165–1173.

Linkov, A.M. 1997. New geomechanical approaches to develop quantitative seismicity. In *Rockbursts and seismicity in mines*, pp. 151–166.

Linkov, A.M. 2002. Integration of numerical modeling and seismic monitoring: general theory and first steps. In *Proceedings of the International Conference on New Developments in Rock Mechanics*, pp. 259–264.

Linkov, A.M. 2006. Numerical modeling of seismic and aseismic events in three dementional problems of rock mechanics. *Journal of Mining Science*, vol. 42, no. 1, pp. 1–14.

Linkov, A., Rybarska-Rusinek, L., Zoubkov, V. 2015. On comparison of simulated and observed seismicity. 07 2015.

Linkov, A., Rybarska-Rusinek, L., Zoubkov, V. 2016. Reasonable sets of input parameters and output distributions for simulation of seismicity. *International Journal of Rock Mechanics and Mining Sciences*, vol. 84, pp. 87–94, 04 2016. doi: 10.1016/j.ijrmms.2016.02.004

Linkov, A.M. 2013. Numerical modelling of seismicity: Theory and applications, Keynote lecture. In A. Malovichko and D. Malovichko, editors, *8th International Symposium on Rockbursts and Seismicity in Mines*, Russia, pp. 197–218.

Malovichko, D. 2020. Description of seismic sources in underground mines: Theory. *Bulletin of the Seismological Society of America*.

Malovichko, D. 2022. Utility of seismic source mechanisms in mining. In *Proceedings of the Tenth International Symposium on Rockbursts and Seismicity in Mines, Society for Mining, Metallurgy & Exploration*, Englewood, 2022.

McGarr, A., Bicknell, J., Sembera, E., Green, R.W.E. 1989. Analysis of exceptionally large tremors in two gold mining districts of south africa. *Seismicity in mines*, pp. 295–307.

Mendecki, A.J., Sciocatti, M. 1997. Seismic Monitoring in Mines, chapter 5, location of seismic events, pp. 87–107.

Mendecki, A.J., Niewiadomski, J. 1997. Seismic Monitoring in Mines, chapter 8, spectral analysis and seismic source parameters, pp. 144–158.

Mendecki, A.J., van Aswegen, G., Mountfort, P. 1999a. A Handbook on Rock Engineering Practice for Tabular HardRock Mines, chapter 9.4, a guide to routine seismic monitoring in mines, quantification of seismic sources, pp. 291–293.

Mendecki, A.J., van Aswegen, G., Mountfort, P. 1999b. A Handbook on Rock Engineering Practice for Tabular Hard Rock Mines, chapter 9.3, a guide to routine seismic monitoring in mines, location of seismic events, pages 290–291.

Mendecki, A.J. 2012. Size distribution of seismic events in mines. In *Proceedings of the Australian Earthquake Engineering Society 2012 Conference*, Queensland, pp. 1–20.

Mendecki, A.J. 2013.Mine Seismology: Glossary of Selected Terms. In *8th International Symposium on Rockbursts and Seismicity in Mines*, pp. 523–550, St Petersburg-Moscow, Russia.

Mendecki, A.J. 2016a. Mine Seismology Reference Book: Seismic Hazard, chapter 3, maximum event size. *Institute of Mine Seismology*, pp. 31–35. ISBN 978-0-9942943-0-2, www.imseismology.org/msrb/, 1 edition, May 2016a. http://www.imseismology.org/msrb/

Mendecki, A.J. 2016b. Mine Seismology Reference Book: Seismic Hazard, chapter 2, power laws and their utility. *Institute of Mine Seismology*, pp. 20–31. ISBN 978-0-9942943-0-2, www.imseismology.org/msrb/, 1 edition, May 2016b. URL http://www.imseismology.org/msrb/.

Motsepe, P.T., Motloba, J.M., Steenkamp, P.W., Lekubo, B.P, Mashego, H.E. 2021. Mineral resources and mineral reserves as at june 2021. Technical report, Harmony Gold, 2. https://www.har.co.za/21/download/HAR-RR21.pdf

Mthenjane, M. 2025. Minerals council south africa facts and figures pocket book 2024. https://www.mineralscouncil.org.za/component/jdownloads/?task=download.send&id=2390&catid=17&m=0&Itemid=119

Napier, J.A.L. 1987. The application of excess shear stress to the design of mine layouts. *Journal of the Southern African Institute of Mining and Metallurgy*, vol. 87, no. 12, pp. 397–405.

Napier, J.A.L., Stephansen, S.J. 1987. Analysis of deep-level mine design problems using the minsim-d boundary element program. In *Proceedings of the Twentieth International Symposium on the Application of Computers and Mathematics in the Mineral Industries.*, vol. 1, pages 3–19.

Napier, J.A.L., Malan, D.F. 2007. The computational analysis of shallow depth tabular mining problems. *Journal of the Southern African Institute of Mining and Metallurgy*, pp. 725–742.

Napier, J.A.L., Daniel Francois Malan. 2011. Numerical computation of average pillar stress and implications for pillar design.

Napier, J.A.L., Malan, D.F. 2012. Simulation of time-dependent crush pillar behaviour in tabular platinum mines. *Journal of the Southern African Institute of Mining and Metallurgy*, pp. 711–719.

Napier, J.A.L., Malan, D.F. 2014. A simplified model of local fracture processes to investigate the structural stability and design of large-scale tabular mine layouts. In *ARMA US Rock Mechanics/Geomechanics Symposium*, pp. ARMA–2014. ARMA.

Napier, J.A.L., Malan, D.F. 2018. Simulation of tabular mine face advance rates using a simplified fracture zone model. *International Journal of Rock Mechanics and Mining Sciences*. https://api.semanticscholar.org/CorpusID:134150957

Napier, J.A.L. Malan, D.F. 2021. A limit equilibrium model of tabular mine pillar failure. *Rock Mechanics and Rock Engineering*, vol. 54, pp. 71–89.

Ortlepp, W.D. 1997. Rock Fracture and Rockbursts: An Illustrative Study. Monograph series. *South African Institute of Mining and Metallurgy*. ISBN 9781874832676. https://books.google.co.za/books?id=tYQQAQAAMAAJ

Ortlepp, W.D. 2000. Study of rockburst source mechanism, gap 524 project. Technical report, *SIMRAC*, Johannesburg

Ortlepp, W., Armstrong, R., Ryder, J., OConnor, D. 2005. Fundamental study of micro-fracturing on the slip surface of mine-induced dynamic brittle shear zones. pp. 229–237, 01 2005. doi: 10.36487/ACG_repo/574_20

Ryder, J.A.E. 1987. xcess shear stress (ess): An engineering criterion for assessing unstable slip and associated rockburst hazards. In *ISRM Congress*, pages ISRM–6CONGRESS. ISRM.

Ryder, J.A. 1988. Excess shear stress in the assessment of geologically hazardous situations. *Journal of the Southern African Institute of Mining and Metallurgy*, vol. 88, pp. 27–39.

Ryder, J.A., Jager, A.J., Lightfoot, N. 1999. A Handbook on Rock Engineering Practice for Tabular Hard Rock Mines, chapter 11.3.5, numerical modelling, displacement discontinuity method, p. 337.

Ryder, J.A. 2002. A textbook on rock mechanics for tabular hard rock mines, chapter 2.6.2, mechanical properties of rock, shear properties of discontinuities, pp. 100–105.

Ryder, J.A., Malan, D.F. 2002. A textbook on rock mechanics for tabular hard rock mines, chapter 4.2.3, analytic solutions in elasticity, boundary element kernels, pp. 164–169.

Ryder, J.A., Jager, A.J. 2002. A textbook on rock mechanics for tabular hard rock mines, chapter 2.3.3, mechanical properties of rock, hoek-brown empirical strength criterion, pp. 68–70.

Ryder, J.A., York, G., Squelch, A.P. 2002. A textbook on rock mechanics for tabular hard rock mines, chapter 6.3, rockmechanics in the design of mining layouts, excess shear stress, pp. 255–267.

Robson, D.S., Whitlock, J.H. 1964. Estimation of a truncation point. *Biometrika*, vol. 51, no. 1/2, pp. 33–39.

Salamon, M.D.G. 1964. Elastic analysis of displacements and stresses induced by mining of seam or reef deposits – part iv: Inclined reef. *Journal of the Southern African Institute of Mining and Metallurgy*, vol. 65, pp. 319–338.

Salamon, M.D.G.,Weibols, G.A. 1972. Location of Seismic Events. Technical report, Chamber of Mines Research Organisation.

Salamon, M.D.G. 1993. Keynote address: Some applications of geomechanical modelling inrockburst and related research. In *3rd International Symposium on Rockbursts and Seismicity in mines*, pp. 297–309.

Starfield A.M., Crouch, S.L. 1973. Elastic analysis of single seam extraction. In *New Horizons in Rock Mechanics, American Society of Civil Engineers,* pp. 421–439.

Stankiewicz, T., Essrich, F. 2004. Standardised local magnitude scale for south african mines. Technical report, AngloGold Ashanti.

Spottiswoodet, S.M. 1988. Total seismicity, and the application of ess analysis to mine layouts. *Journal of the Southern African Institute of Mining and Metallurgy*, vol. 88, no. 4, pp. 109–116.

Spottiswoode, S.M. 2009. Is mine earthquake prediction possible. Rockbursts and Seismicity in Mines, Dalian, China.

Spottiswoode, S.M. 2010. Mine seismicity: Prediction or forecasting? *Journal of the South African Institute of Mining and Metallurgy*, vol. 110, no. 1, pp. 11–20.

Tucker, R.F., Viljoen, R.P., Viljoen, M.J. 2016. A review of the witwatersrand basin the worlds greatest goldfield. *Episodes*, vol. 39, no. 2, pp. 105–133.

van der Wath, S., Mohlatsane, J., Gerber, J.D. 2022. Seismic source mechanism characteristics observed during the bambanani mine shaft pillar extraction. Technical report, Association of Mine Managers South Africa.

Van Der Wath, S. 2023. Digitized mining steps and faults associated with the shaft pillar extraction at bambanani mine, supplied by harmony gold.

Van Aswegen, G. Ortlepp. 2008. Shears - dynamic brittle shears of South African gold mines. *Proc. 1st SHIRM Symposium*, 2, pp. 111–119, 01.

Van Aswegen, G. 2003. Towards best practice for routine seismic hazard assessment in mines. *The Southern African Institute of Mining and Metallurgy*.

Van Aswegen, G. 2005. Routine seismic hazard assessment in some south african mines. In *Controlling Seismic Risk: Sixth International Symposium on Rockburst and Seismicity in Mines Proceedings*, 9-11 March 2005, Australia, p. 437. Australian Centre for Geomechanics.

Van Aswegen, G. 2020. Fault stability in sa gold mines. In *Mechanics of Jointed and Faulted Rock*, pp. 717–725. CRC Press.

Van Aswegen, G., Stander, M. 2012. Origins of some fractures around tabular stopes in deep south african mines. *Journal of the Southern African Institute of Mining and Metallurgy*, vol. 112, no. 8, pp. 729–735.

Van Aswegen, G. 2013. Forensic rock mechanics, ortlepp shears and other mining induced structures. In *8th International Symposium Rockburst and Seismicity in Mines*, Saint-Petersburg, Moscow, pages 47–51.

Van Aswegen, G. 2021a. Forensic rock mechanics for the analysis of rockbursts and seismicity in mines, lecture series for south african rock mechanics practitioners, lecture 1, sections 6 and 7, nature of deformation controlled by rock characteristics and shear zones. https://www.sanire.co.za/images/fbfiles/GvA-webinar-20210707-f-lo-res-2.pdf

Van Aswegen. G. 2021b. Forensic rock mechanics for the analysis of rockbursts and seismicity in mines, lecture series for south african rock mechanics practitioners, lecture 2, section 4, rockburst nomenclature. https://www.sanire.co.za/images/fbfiles/GvA-20210721-A-fin-02082021.pdf